CHAPTER - 9

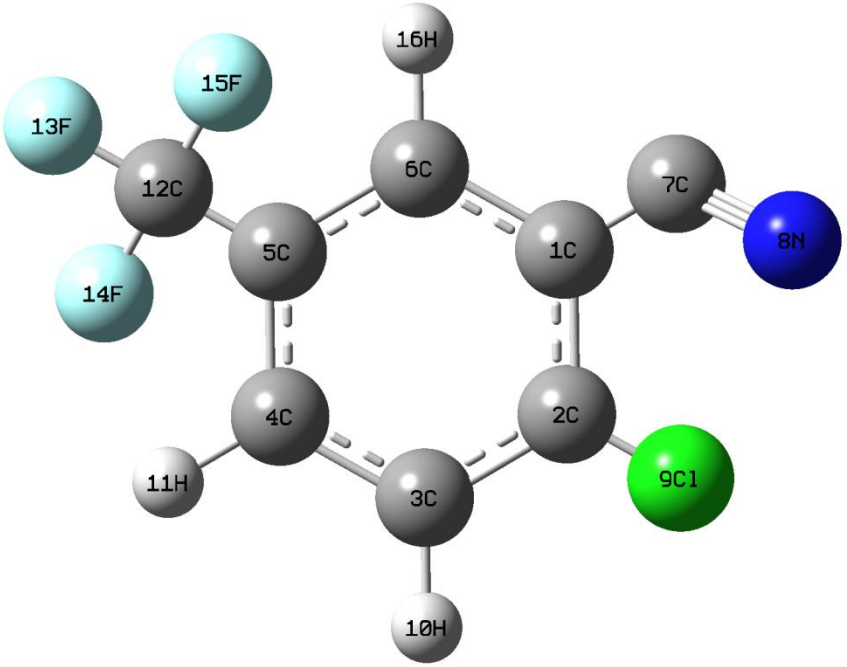

SYNTHESIS AND SPECTROSCOPIC CHARACTERIZATION OF 2-CHLORO-5-(TRIFLUOROMETHYL) BENZONITRILE AN EXPERIMENTAL AND THEORETICAL APPROACH

CHAPTER – 9

9.1 INTRODUCTION

Benzonitrile is a clear colorless liquid with an almond like odour and its Flash point 161°F. Benzonitrile is less soluble in water, which is used as a special solvent to make other chemicals.It is considered as chief solvent, that acts as a chemical transition for the synthesis of dyestuffs, pharmaceuticals and rubber chemicals through the process of alkylation, condensation, esterification, hydrolysis, halogenation or nitration and as well, a versatile precursor to many of the derivatives.Benzonitrile derivatives are used in the process of polymers, lacquers and anhydrous metallic salts as well as intermediates for agrochemicals, pharmaceuticals and other organic chemicals. 4-Hydroxybenzonitrile is an insecticidal (Fukuto., 1956) and antifungal (Tsuda *et al.,* 1983) agent and its toxicity has been studied repeatedly (Kaiser *et al.,* 1983; Claw *et al.,* 1983; Schultz., 1987).

4-Acetylbenzonitrile finds usage in synthetic organic and pharmaceutical industry.4-Formylbenzonitrile is as an intermediate for organic synthesis, liquid crystals and pharmacy. Benzonitrile can form coordination complexes with transition metals that are both soluble in organic solvents and conveniently liable. The benzonitrile ligands are readily displaced by stronger ligands, making benzonitrile complexes useful synthetic intermediates (Anderson., 1990). The benzonitrile molecule and some of its derivatives have been studied because of their interesting biochemical and physical properties (Konishi*et al.,* 2001; Raap*et al.,* 1999; Dini., 2000; Koti and Periasamy., 2002). The ab initio force field computations of 4-hydroxybenzonitrile were performed by the Games software (Binev, 2001).

Dimitrova has studied the vibrational spectra of benzonitrile and its radical anion (1997), the molecular structure and vibrational properties of 2-formylbenzonitrile (Misra*et al.,* 2007) and 3-chloro-4-fluorobenzonitrile (Balachandran and Parimala., 2013), 4-bromobenzonitrile (Krishnakumar., 2009), 4-(dimethylamino)benzonitrile and its isotopomers (Okamoto*et al.,* 2000), 4-(1H-pyrrol-1-yl)benzonitrile and 5-cyano-2-(1-pyrrolyl)pyridine (Schweke., 2007) were carried out. From a theoretical point of

view, 4-acetylbenzonitrile,4-formylbenzonitrile and 4-hydroxybenzonitrile molecules are interesting because it contains different binding sites for its interaction with the metal surface and it contains an aromatic ring, the CN group,and isolated pair of electrons on nitrogen and oxygen atoms (Loo*et al*., 1985).

Hence in the present work, vibrational spectra and electronic structure properties of 2-Chloro-5-(trifluoromethyl)benzonitrile (TFMBN) was studied. DFT calculations have been performed about title compound. Thus, the experimental and theoretical studies of TFMBN molecule, important conjugated compounds of biological and industrial interest, have been reported in this investigation. Density functional theory (DFT) have been employed in the investigation to provide the structural properties of the title molecule using B3LYP with 6-311++G (d,p) basis set. The theoretical results are compared with experimental data, in order to dig out more information on the depiction of molecular properties.

9.2 METHODOLOGY

9.2.1. Material Synthesis

The Chemical Production at Sigma-Aldrich chemicals, USA have produced 2-chloro-5-(trifluoromethyl)benzonitrile (I) (Scheme 1).The product is a key intermediate in the production of the anti-psychotic drugs Fluanxol and Fluanxol Depot (III and II) (Scheme 2).

Recently, it was decided to reevaluate the process to develop a procedure suitable for scale-up and moreover to improve the personal safety for the operators performing the reactions.In connection with the scale-up, a process safety evaluation was performed.2-Chloro-5-trifluoromethyl-benzonitrile is formed by a Sandmeyer reaction of 2-chloro-5-trifluoro methylaniline (V) with sodium nitrite in the aqueous form of sulfuric acid. The formed diazonium salt (IV) is then reacted with a mixture of copper-(I) cyanide and sodium cyanide in the presence of sodium carbonate to afford the desired product (Scheme 3).The reaction scheme is given in Figure 9.1.

In the current procedure, developed in the early 1970s, four batches of the diazonium salt solution were produced by mixing V (2.0 kg) with ice (4 L) and concentrated sulfuric acid (1.3 L) in an open container (28 L). After stirring for 30 min,

sodium nitrite (0.8 kg) dissolved in water was added to the container, which was cooled to -2 to +2 °C by addition of ice. The procedure was performed in a large scale hood.

The four batches were filtered on a steel nutsche filter,and the combined filtrates were added to sodium carbonate(12 kg), copper cyanide (3.8 kg), and sodium cyanide (3.2kg) suspended in water (30 L) in a 250-L reactor.After stirring for 2 h, the heptane was added to the mixture, and the phases were separated. A small volume of inter phase emulsion was filtered on a steel nutsche filter and the recovered aqueous phase returned to the heptane phase.

This procedure was repeated five times (giving a total of 10 diazonium batches), and the combined heptane phases were washed with hot water.After evaporation to dryness the product (I) was distilled under reduced pressure. It takes about 5 days to produce one batch to give a yield of 25 kg/week.

9.3 COMPUTATIONAL DETAILS

The molecular structure of TFMBN in the ground state is optimized by utilizing Becke's three parameter hybrid functional (B3) (Becke., 1988; 1993) combined with gradient corrected correlation functional of Lee-Yang-Parr(LYP) (Lee *et al.*, 1988) with high level triple zeta 6-311++G (d,p) basis set using Gaussian 09W program (Denningto*et al*., 2008; Frisch *et al.*, 2000)to characterize molecular structure optimization, vibrational frequencies, thermodynamic properties and energies of the optimized structures. The optimized parameters of the compound TFMBN was used for harmonic vibrational frequency calculations resulting in FT-IR and FT-Raman frequencies together with intensities, Raman activities and the force constants obtained from B3LYP/6-311++G (d,p) method.

The total energy distribution corresponding to each of the observed frequencies shows the reliability and accuracy of the spectral analysis. By combining the results of the Gauss view's program (Frisch *et al.,* 2000) with symmetry considerations,vibrational frequency assignments were made with a high degree of accuracy.The force field transformation and subsequent normal coordinate analysis and computation of the total energy distribution (TED) were performed on a PC with the MOLVIB program (Version 7.0-G77) proposed by Sundius (2002). Nonlinear optical

(NLO) and thermodynamic properties of TFMBN have been calculated by the same level of theory.

The natural bonding orbital (NBO) calculation (Glendening*et al.*, 1988) were performed using NBO3.1 program as implemented in Gaussian 09W (Frisch *et al.*, 2000) package at B3LYP method in order to understand various second order interactions between the another subsystem, which is a measure of the intramolecular delocalization or hyper conjugation. NMR Chemical shielding anisotropy parameters are calculated using B3LYP level with same basis set.

9.3.1. Prediction of Raman Intensities

The Raman activities (S_i) calculated with the Gaussian09W software (Frisch *et al.*, 2000) are converted to relative Raman intensities (I_i) using the following relationship derived from the basic theory of Raman scattering (Chocholousova*et al.*, 2004);

$$I_i = \frac{f(\nu_0 - \nu_i)^4 s_i}{\nu_i \left[1 - \exp\left(\frac{-hc\nu_i}{k_b T}\right)\right]} \qquad (9.1)$$

Where ν_i is the vibrational wavenumbers of the i^{th} normal mode, ν_0 is the exciting frequency (in cm^{-1} units), h, c, and k_b are universal constants, T is the temperature and f is the suitably chosen for common scaling factor for all the peak intensities.

9.4 RESULTS AND DISCUSSION

9.4.1 Molecular Structure

The molecular structure of the TFMBN belongsto C1 point group symmetry and the optimized molecular structure of title molecule is shown in Figure 9.2 along with the atom numbering.The title molecules have got 16 atoms, and it possesses 42 fundamental vibrational modes as 29 in-plane vibrations and 13 out-of-plane vibrations. A molecule consists of 8 C atoms, 1 N atom, 1 Cl atom, 3 H atoms and 3 F atoms constitute in selected molecule.Thevibrations predicted in the molecule were all active in both FT-IR and FT-Raman.

9.4.2 Vibrational Spectral Analysis

The comparison between the observed FT-IR and FT-Raman spectral frequencies of TFMBN with calculated FT-IR and FT-Raman spectral wave numbers has been done in Figures 9.3 and 9.4. The complete description of experimental FT-IR and FT-Raman spectra is presented in Table 9.1 along with the comprehensive assignment as stipulated by TED. The scaled vibrational frequencies were well correlated with experimental vibrational frequencies.Some of the bands in theoretically calculated FT-IR are missing in experimental FT-IR due to the coexistence of broader and larger bands.The observed and calculated vibrational assignments frequencies for various functional groups are conversed below.

9.4.3 C–H Vibrations

Normally, the ring C–H stretching vibration is expected in the region 3500–3000 cm^{-1} (Peter., 2011). Out of the three expected C–H stretching vibration modes,1, 2 and 3 are observed as weak and very weak bands in FT-IR spectrum at 3500 and 3250 cm^{-1} whereas mode 3 is in active in FT-Raman. Normal vibrations 16, 17 and 19 are characterized by C–H in-plane bending vibrations of trisubstituted benzene derivatives. The mode 3 is of both IR and Raman inactive but occurs in the region about 1300 cm^{-1} (Varsanyi., 1974) C–H in-plane bending mode 3 is inactive in IR and inRaman but the scaled value is at 1185 cm^{-1}. The mode 16 and 19 occurring more close to 1250, 1020 cm^{-1} is observed in FT-IR as strong bands and three modes observed as very weak and medium bands at 1250, 1200 and 1040 cm^{-1}in FT-Raman spectrum. The theoretically computed C–H in-plane bending vibrations are 1193, 1127 and 945 cm^{-1}show excellent agreement with experimental observation.The C–H in-plane bending modes and out-of-plane bending vibrations of TFMBN are assigned in the characteristic region.

9.4.4 Ring Vibrations

The aromatic C–C stretching vibration occurs in the region 1589–1301 cm^{-1} (Peter, 2011). In the present study, the wavenumbers observed at 1750 (vs), 1700(m), 1580(s), 1500(vs) cm^{-1} in the FT-IR spectrum, 1980(vs), 1420(s) cm^{-1} in the FT-Raman spectrum and 1813-1329 cm^{-1} values are calculated theoretically assigned to C–C stretching vibrations.It shows the theoretical values good agreement with experimental data. As expected, the in-plane deformations were observed at higher frequencies than

the out-of-plane vibrations. The in-plane and out-of-plane bending modes are also good agreement with experimental data.

9.4.5 CF_3 Vibrations

Usually symmetric and asymmetric CF_3 stretching vibrations are in the ranges 1270-1235 $cm^{-1}$and 1226-1200 cm^{-1}, respectively (Parimala and Balachandran, 2011; Fernandez*et al.,* 2002). The CF_3 group asymmetric and symmetric stretching vibrations are inactive both FT-IR and FT- Raman spectra and the same 2815, 2729 and 2658 cm^{-1} theoretically calculated by B3LYP method.The CF deformation vibrations usually occur in the regions 690–631 cm^{-1}, 640–580 $cm^{-1}$and 590–490 cm^{-1} (Socrates., 2001). Accordingly, CF_3 ipb and CF_3 opb vibrations are identified at 1100 cm^{-1} in FT-IR spectrum and 1180 and 940 cm^{-1} in FT-Raman spectrum of TFMBN. The above are supported by the literature (Gounev *et al.,* 1997; Tuttolomondo*et al.,* 2004). The band obtained at 800 cm^{-1}in FT-IR spectrum is assigned to CF_3 out-of-plane rocking mode. It is difficult to observe the torsional motion in the spectra. This is partly because of the low wave number of the CF_3 torsional absorption and to the strong intensities of the rotational bands.

9.4.6 C–Cl Vibrations

In benzene derivatives containing a Cl atom, the C–Cl stretching frequency appears in the region 800–600 cm^{-1} (Varsanyi., 1974; Singh and Shamir., 1977).The frequency 823 cm^{-1} is theoretically calculated and assigned to the C–Cl stretching mode.The C–Cl deformation mode with wavenumbers expected below 400 cm^{-1}(Faniran., 1981) is rather difficult to assign in 2-A, 5-CB; firstly, because the most Raman spectral lines are weak in the region and secondly, because the IR range does not go beyond 200 cm^{-1}. In the present case, a very weak FT-Raman band at 390 cm^{-1} is assigned to the C-Cl in-plane bending mode. In the present case, C-Cl out-of-plane bending modes are well within the expected ranges suggested by Varsanyi (1974).

9.5 NON-LINEAR OPTICAL (NLO) PROPERTIES

NLO studies find wide applications in laser technology, optical communication, optical information processing. NLO is at the forefront of current research due to its importance in providing key functions of frequency shifting, optical modulation,

switching, laser, fiber, optical materials logic and optical memory for the emerging technologies in areas such as telecommunications, signal processing and optical inter connections (Datta and Pati., 2003; Govindarajan and Karabacak., 2012; Saravanan *et al.,* 2017). The possible application of the TFMBN in the field of non-linear optics dmand for the assessment of its structural and bonding characteristics causative to the hyperpolarizability improvement by evaluating the vibrational modes with the help of FT-IR and FT-Raman spectroscopy.

For calculating hyperpolarizability, the geometry of the investigated molecule is treated as an isolated molecule. The optimization has been carried out in the unrestricted open-shell B3LYP level. The geometries are fully optimized without any constraint with the help of analytical gradient procedure implemented within Gaussian 09W program (Frisch *et al.,* 2008). The electric dipole moment and the dispersion free first hyperpolarizability are calculated using finite field method. The finite field method offers a straight forward approach to the calculation of hyperpolarizability (Krishnakumar and Nagalakshmi, 2008).

In the presence of an applied electric field, first order hyperpolarizability is a third rank tensor that can be described by a 3x3x3 matrix. The requisite for 3D matrix components can be deduced to 10 components because of the kleinman symmetry (Kleinman, 1962). The matrix can be given in the lower tetrahedral format and it is obvious that the lower part of the 3x3x3 matrixes is a tetrahedral.

The sum total of the static dipolemoment (μ), the anisotropy polarizability ($\Delta\alpha$), the average polarizability (α_0), first hyperpolarizability (β_0) and vector hyper polarizability (β_{vec}) using the x, y, z components are defined in terms of the equation as follows:

$$\mu = \left(\mu_x^2 + \mu_y^2 + \mu_z^2\right)^{1/2} \tag{9.2}$$

$$\alpha_0 = \frac{1}{3}\left(\alpha_{xx} + \alpha_{yy} + \alpha_{zz}\right) \tag{9.3}$$

$$\Delta\alpha = \frac{1}{\sqrt{2}}\left[\left(\alpha_{xx} - \alpha_{yy}\right)^2 + \left(\alpha_{yy} - \alpha_{zz}\right)^2 + \left(\alpha_{zz} - \alpha_{xx}\right)^2 + 6\alpha_{xz}^2 + 6_{xy}^2 + 6\alpha_{yz}^2\right]^{\frac{1}{2}} \tag{9.4}$$

$$\beta_0 = \left[\left(\beta_{xxx} + \beta_{xyy} + \beta_{xzz} \right)^2 + \left(\beta_{yyy} + \beta_{yzz} + \beta_{yxx} \right)^2 + \left(\beta_{zzz} + \beta_{zxx} + \beta_{zyy} \right)^2 \right]^{\frac{1}{2}} \quad (9.5)$$

$$\beta_{vec} = \frac{3}{5} \left[\left(\beta x^2 + \beta y^2 + \beta z^2 \right)^{1/2} \right] \quad (9.6)$$

The $\beta_0$components of Gaussian output are reported in atomic units and therefore the calculated values are converted into esu units (1 a.u=8.3693×10^{-33}esu). The calculated values of hyperpolarizability and polarizability are tabulated in Table 9.2. According to the present calculations, the total molecular dipole moment (μ=8.548 Debye), the anisotropy of the polarizability (Δα=18.615×10^{-24}), polarizability (α_0=–47.643×10^{-24}esu) and the first hyperpolarizability (β_0=8.179×10^{-24}esu), vector hyper polarizability (β_{vec}=5.358×10^{-24}esu) for TFMBN molecule by B3LYP method with 6-311+G (d,p) basis set.

9.6 NATURAL BOND ORBITAL (NBO) ANALYSIS

Natural bond orbital (NBO) analysis provides the most accurate possible "natural Lewis structure" and all orbital details are mathematically chosen to include the highest possible percentage of the electron density. The potential aspect of the NBO method is that it provides information about interactions in both filled and effective orbital spaces that could enhance the analysis of intra and intermolecular interactions.

The second-order Fock matrix was carried out to evaluate the donor–acceptor interactions in the NBO analysis (Glendening*et al.,* 1988). The resut of interaction is a loss of occupancy from the localized NBO of the idealized Lewis structure into an empty non-Lewis structure. For the each donor (i), acceptor (j) and the stabilization energy $E^{(2)}$associated with the delocalization i→j is estimated as

$$E^{(2)} = -n_\sigma \frac{\langle \sigma | F | \sigma \rangle^2}{\varepsilon_{\sigma^*} - \varepsilon_\sigma} = -n_\sigma \frac{F_{ij}^2}{\Delta E} \quad (9.7)$$

Where $\langle \sigma | F | \sigma \rangle^2$ or F_{ij}^2 is the Fock matrix element between the i and j NBO orbital, ε_{σ^*} and ε_σ are the energies of σ and σ* NBO's and n_σ is the population of the donor σ orbital.

NBO analysis has been performed to enlighten the charge transfer or delocalization of charge owing to the intramolecular interaction among the bonds and also supplies a convenient basis for investigating a conjugative interaction or charge

transfer in molecular systems. Some electron donor orbital, acceptor orbital and the interacting stabilization energy resulting from the second order micro disturbance theory is reported (Reed *et al.,* 1988; Kalinowski *et al.,* 1988). The higher the stabilization energy value, the more productive is the interaction between electron donors and electron acceptors, i.e. the higher the tendency of donating electrons from electron donors to electron acceptors and larger the extent of conjugation of whole system.

Delocalization of the density of electron between occupied Lewis-type (bond or lone pair) NBO orbitals and officially unoccupied (anti-bond or Rydberg) non-Lewis type NBO orbitals that correspond to a stabilizing donor-acceptor interaction.NBO calculation is performed using Gaussian09W package program at the B3LYP level in order to elucidate several second order interactions between the filled orbital of one subsystem and vacant orbital of another subsystem, which is a measure of thedelocalization or hyperconjugation. The corresponding results have beenpresented in Tables 9.3 and 9.4.

The intramolecular interactions are observed as increase in electron density (ED) in (C–N) anti-bonding orbital that weakens the respective bonds. The electron density of conjugated bond of substitution (1.988 a.u) clearly demonstrates strong delocalization. The occupancy of π bonds is lesser than σ bonds which lead more delocalization.

The intramolecular hyperconjugative interaction of the distributed σ electrons of σ*(C5–C6) to the anti σ*(C1–C2) bond in the ring leads to stabilization of some part of the ring as evident from Table 8.4. The intramolecular hyperconjugative interaction of the σ(C2–Cl9) to the anti σ*(C2–C1) and σ*(C2–C3) bonds in the ring leads to stabilization of 5.97 and 4.69 KCal/mol.

9.7 ANALYSIS OF NMR SPECTRUM

For the structural analysis of organic compound, chemical shift analysis is one of the most important techniques. ^{13}C and ^{1}H NMR chemical shifts calculations of optimized molecule was carried out by Gauge Independent Atomic Orbital (GIAO) and B3LYP method with 6-311+G (d,p) basis set. The experimental and calculated values of ^{13}C and ^{1}H NMR chemical shifts are given in Table 9.5. Agreement between theory and experiment is inconsistent, sometimes good and sometimes poor. Both experimental and theoretical results are in agreement expected for the proton of the CN group in case of

^{13}C NMR of TFMBN. The ^{1}H NMR spectrum of the title compound is measured in the medium of $CDCl_3$. ^{1}H NMR spectra observed for title molecule is given in Figure 9.5 The aromatic ring protons in the ^{1}HNMR spectrum of the title molecule appeared at 7.2–6.8 ppm that represent the benzene ring. The ^{13}C NMR spectrum showed signals that observed 124–70 ppm in $CDCl_3$ and they calculated the corresponding shifts in 129.496–82.943 ppm by B3LYP/6-311+G(d,p) level of theory.

9.8 THERMODYNAMIC PROPERTIES

On the basis of vibrational analysis, the statically thermodynamic functions: heat capacity (Cp), enthalpy changes (H–E/T), Gibb's free energy (G–E/T) and entropy (S) for the TFMBN molecule were obtained from the theoretical frequencies and listed in Table 9.6. From the Table 9.6, it can be observed that these thermodynamic functions are increasing with temperature ranging from 100 to 1000 K due to the fact that the molecular vibrational intensities increase with temperature except Gibb's free energy. The correlation coefficients of entropy, enthalpy changes, heat capacity, Gibb's free energy and temperatures were best fitted by quadratic formulas and the equivalent fitting factors (R^2) for these thermodynamic properties are 0.997, 0.999, 0.998 and 1.000, respectively. The corresponding fitting equations (8–11) are as follows and the correlation graphics of those shown in Figure 9.6.

$$Cp=3.234+0.301T-0.008T^{2}\left(R^{2}=0.999\right) \tag{9.8}$$

$$\left(H-E\right)/T=0.574+0.265T-0.006T^{2}\left(R^{2}=0.999\right) \tag{9.9}$$

$$\left(G-E\right)/T=-56.69-0.132T-0.003T^{2}\left(R^{2}=0.999\right) \tag{9.10}$$

$$S=57.19+0.281T-0.004T^{2}\left(R^{2}=1.000\right) \tag{9.11}$$

All the data interpreted in thermodynamics are effective and that can be taken to the further analysis on the TFMBN. The interpreted data is used to compute certain other thermodynamic energies related to the association of the thermodynamic functions and to calculate approximately the directions of chemical reactions according to the second law of thermodynamics in thermodynamical field.

9.9 REACTIVE DESCRIPTORS

The condensed Fukui functions (f_k) were calculated by simple procedure (based on Mulliken population analysis) given by Yang and Mortier (1986). For a system of N electrons, independent calculations are to be made for corresponding N+1, N–1 and N are total electrons present in anion, cation and neutral state of molecules respectively. Muilliken population analysis yields (gross charges) $q_k(N+1)$, $q_k(N-1)$, $q_k(N)$ and for all atoms k. In a finite-difference approximation, the condensed Fukui functions were given by the equations:

For nucleophilic attack, $f_k^+ = q_k(N+1) - q_k(N)$ (9.12)

Forelectrophilic attack, $f_k^- = q_k(N) - q_k(N-1)$ (9.13)

For free radical attack, $f_k^0 = \frac{1}{2}[q_k(N+1) - q_k(N-1)]$ (9.14)

The condensed-to-atom quantity, ω_k^α corresponding to local elecrophilisity index ($\omega(r)$) was obtained as described previously (Chattaraj *et al.*, 2003):

$$\omega_k^\alpha = \omega f_k^\alpha \quad (9.15)$$

Where α = +, –and 0 refer to nucleophilic, electrophilic and free radical reactions, respectively.

9.10 LOCAL REACTIVITY INDICES-CONDENSED FUKUI FUNCTIONS AND ELECTROPHILISITIES

The information regarding Fukui function (FF) on the confined site reactivity within the molecule and as such, it gives a system for accepting the chemical reactions. These values correspond to the descriptors of reactivity of different atoms in the molecule. As it was mentioned above the presence of substituent (trifluoromethyl or chlorine) linked to (C) atom provokes asymmetry in TFMBN fragment. Thus, different substituents will produce smaller or larger differences between the charges of the trifluoromethyl or chlorine atoms. To point out to the most probable sites, the

condensed Fukui functions [f_k^+, f_k^- and f_k^0 (according to eqns. 9.12–9.14 using Mulliken atomic charges)] were calculated and discussed.

The values reported in Table 9.7, in the reactivity order for the nucleophilic attack, the reactivity of C2 in the chlorine group was found to have a loss in TFMBN. The nucleophilic reactivity order was F15>F14>H10>Cl9>H16>C12>N8>H11>C1>C4>C6>C2. Note, it was observed as a less reactivity for this kind of attack in comparison with the electrophilic attack. On the other hand, the reactivity order for the electrophilic case was C3> F13> C5> C2> C4> C6> C7. Note that the positions of reactive electrophilic sites are different in title molecule and they are mainly located in the ring substitutions, however, due to steric effects, the reactivity in the ring might be difficult.

The attack for free radicals was F15>F14>C12>N8>Cl9>H16>H11>H10>C1. It is evident that the reactivity diminishes in comparison with the more stable than the other atoms. If one compares three kinds of attacks it is possible to observe that in 6-311+G(d,p) basis set the electrophilic and free radical attacks are equivalent and it shows a smaller reactivity in comparison with the nucleophilic case. The results suggest that the degradation TFMBN can be performed by employing either free radical agents or electrophilic agents in order to attack the lateral chain.

9.11 CONCLUSION

The structural and some spectroscopic properties of TFMBN is synthesized in this work are identified by performing the measurements of FT-IR, FT-Raman NMR (^{13}C and ^{1}H) spectra and accomplishing their calculations based on B3LYP method with 6-311+G(d,p) basis set. In addition, the NLO and NBO analyses have been conducted to predict the possible optical properties as well as intra- and intermolecular interactions for studied compound. Here, it is a potential need that the recorded and simulated FT-IR, FT-Raman spectral data of the title molecule is in good terms with each other. The positions of hydrogen and carbon atoms of TFMBN are determined by means of the calculated ^{13}C and ^{1}H NMR chemical shifts as well as corresponding experimental values.

The energy of weak interactions in the molecule and non linear optical properties were studies and reveal the first hyperpolarisability (β_{tot}) of the crystal is

about 16 times that of the reference urea. NBO analysis has shown that for all conformers of present compound, the resonance interaction has mainly contributed to molecular stability but there is also the hyperconjugative interaction ($\sigma \rightarrow \sigma^*$) among the intramolecular interactions contributing to the lowering of the stabilization energy.The association between the temperature and statistical thermodynamics were also found. It was seen that the heat capacity, entropy,enthalpy and Gibb's free energy increase with the increasing temperature owing to the intensities of the molecular vibrations increase with increasing temperature. The local reactivity descriptors (f_k^+, f_k^- and f_k^0) indicate the site for electrophilic and nucleophilic attack.

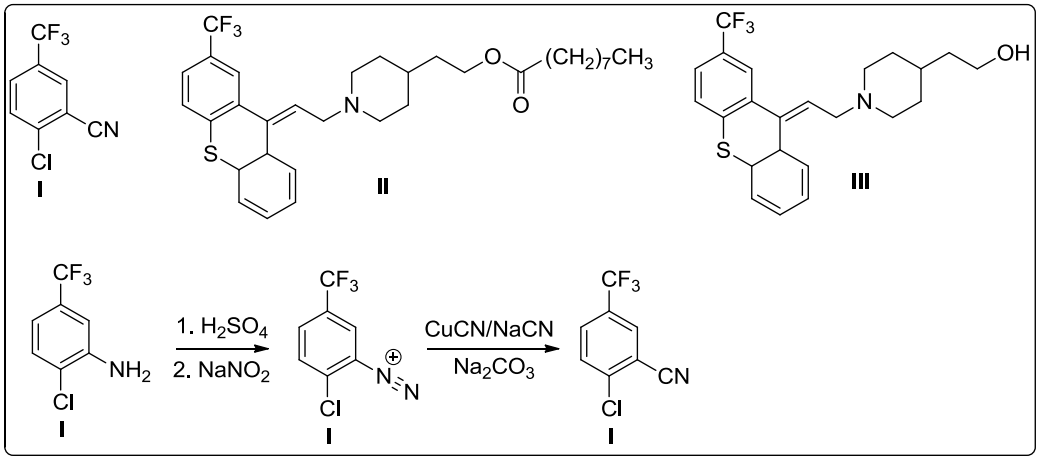

Figure 9.1 Reaction scheme of TFMBN compound

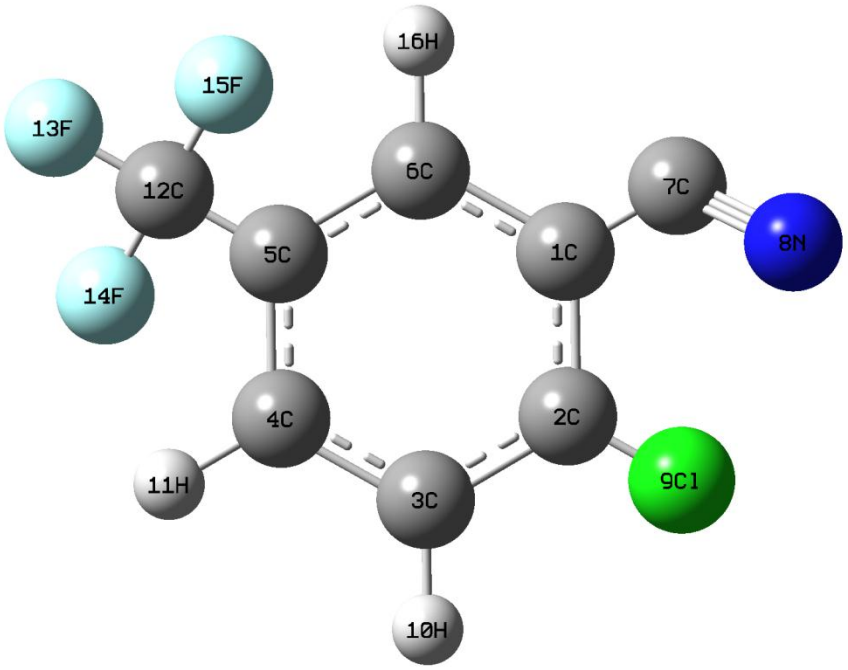

Figure 9.2 The optimized structure of TFMBN

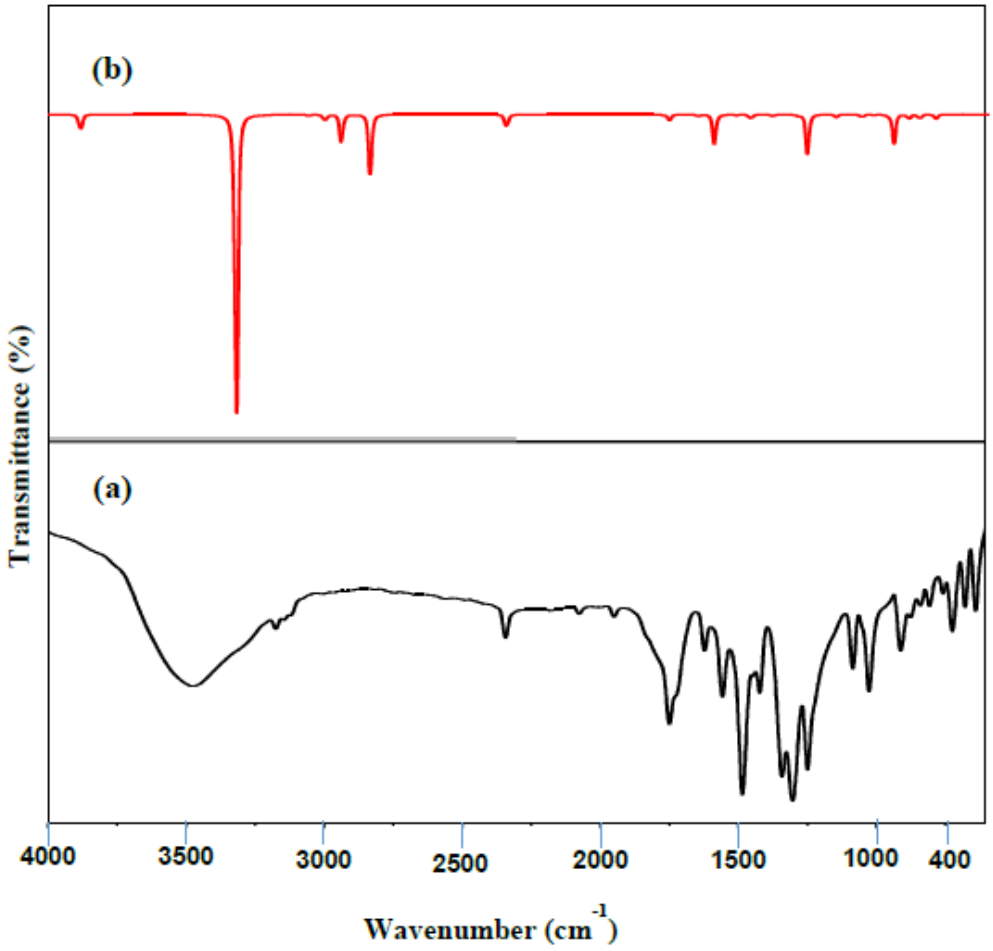

Figure 9.3 FT-IR spectrum of TFMBN (a) experimental and (b) calculated

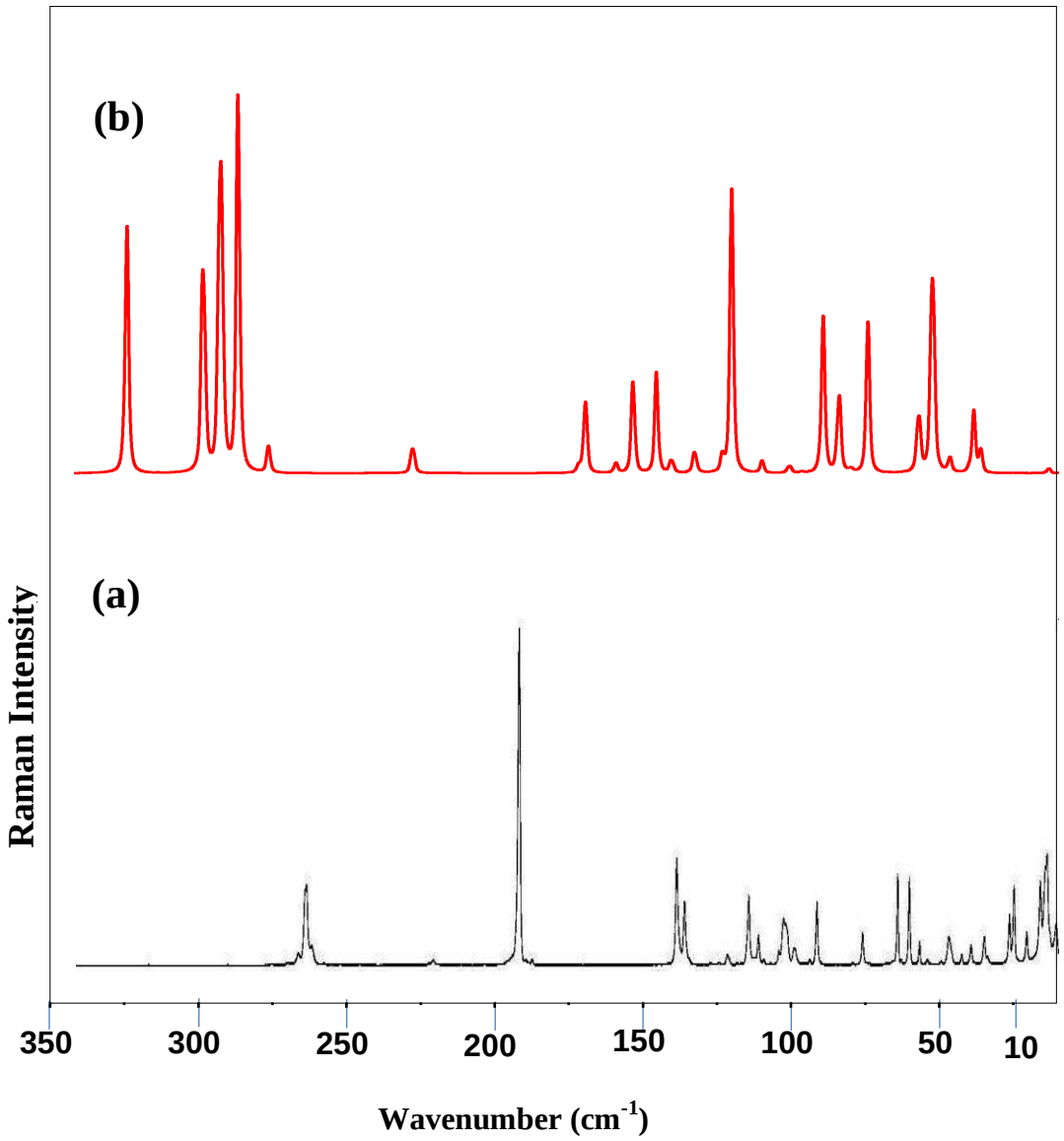

Figure 9.4 FT-Raman spectrum of TFMBN (a) experimental and (b) calculated

(a)

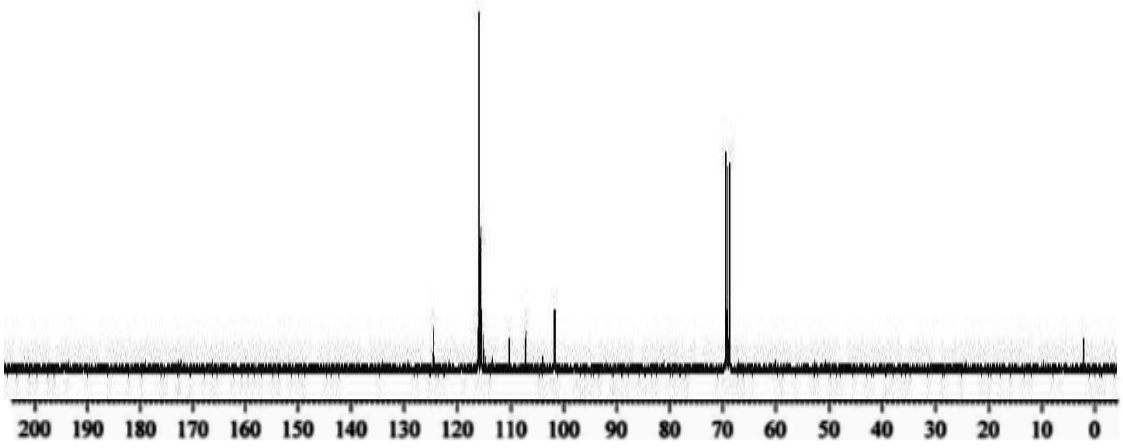

(b)

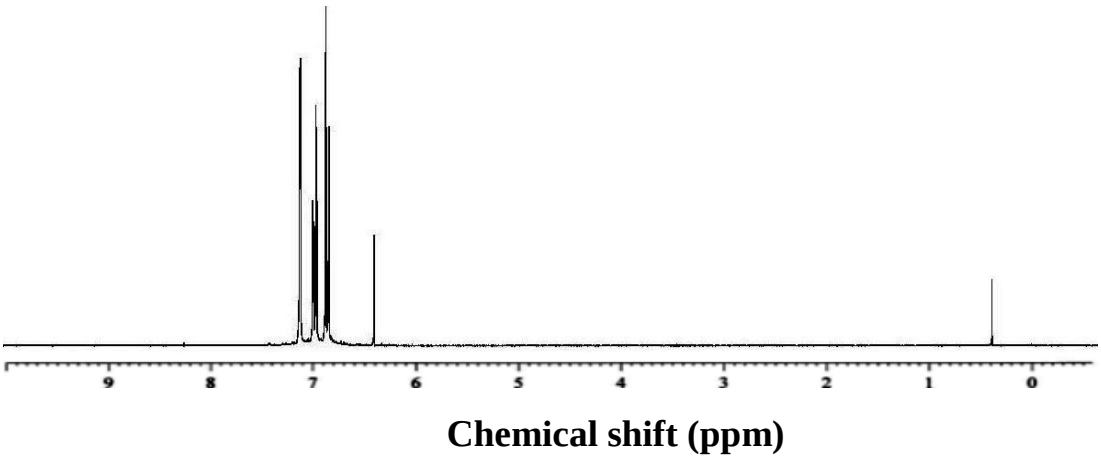

Figure 9.5 (a) The experimental ^{13}C NMR spectrum of TFMBN

(b) The experimental ^{1}H NMR spectrum of TFMBN.

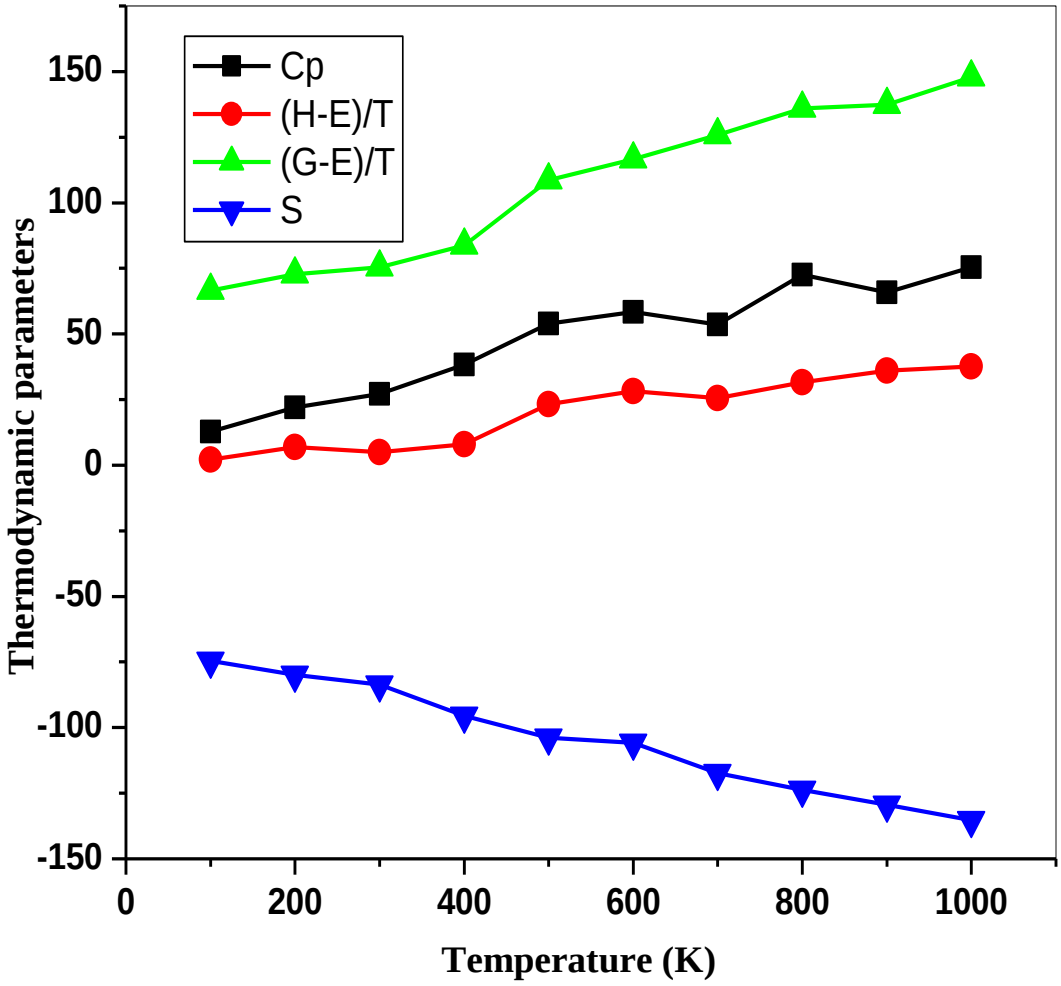

Figure 9.6 Correlation Graphs of Heat Capacity, Entropy, Enthalpy and Gibbs Free Energy calculated at various temperatures using B3LYP/6-311++G(d,p) level of theory.

Table 9.1 Vibrational assignments of fundamental frequencies are obtained for TFMBN using B3LYP/6-311++G(d,p) level of theory.

Sl. No.	Observed frequencies (cm^{-1})		Calculated frequencies (cm^{-1})		IR intensity	Raman intensity	Vibrational assignmentswith >10 % of TED
	FT-IR	FT-Raman	Unscaled	Scaled			
1	3500(w)		3558	3478	120	56	νC–H (100)
2	3250(vw)		3297	3129	262	23	νC–H (99)
3			3036	2945	10	24	νC–H (98)
4			2983	2815	14	64	CF3 asym (89)
5			2974	2729	32	100	CF3 asym (84)
6			2918	2658	192	74	CF3 sym (83)
7		1980(vs)	1914	1813	426	12	νC–C (85)
8			1824	1754	106	13	νC–C (83)
9	1750(vs)		1760	1673	3	2	νC–C (81)
10	1700(m)		1737	1594	41	26	νC–C (81)
11			1634	1517	11	3	νC–C (80)
12	1580(s)		1574	1423	200	29	νC–C (75)
13	1500(vs)		1495	1384	4	30	νC–C (74)
14		1420(s)	1444	1329	33	5	νC–C (72)
15	1380(vw)	1400(m)	1365	1256	11	8	νC–N (76)
16	1250(s)	1250(vw)	1270	1193	8	5	bC–H (71)
17		1200(m)	1239	1127	260	81	bC–H (73)
18	1100(m)	1180(w)	1136	1093	17	3	CF3 ipb (68)
19	1020(s)	1040(vw)	1043	945	21	3	bC–H (63)
20			1001	823	2	4	νC–Cl (64)
21		940(m)	946	792	9	3	CF3 opb (53)
22			928	735	188	41	CF3 sb (54)
23			874	695	30	26	CF3 ipr (52)
24	800(m)		835	641	31	1	CF3 opr (50)
25		780(w)	776	611	25	38	ωC–H (59)
26	600(vw)	620(s)	603	572	9	19	ωC–H (53)
27		590(vw)	556	523	5	70	bC–C (78)
28		490(w)	497	485	15	4	ωC–H (59)
29			432	445	8	7	bC–C (78)
30	400(m)		416	402	12	14	bC–C (67)
31		390(vw)	392	345	8	5	bC–Cl (78)
32			361	302	1	1	bC–C (78)
33			345	284	2	3	bC–C (67)
34			315	242	24	16	bC–N (78)
35			300	205	8	3	ωC–C (57)
36			283	191	16	19	ωC–C (55)
37			265	162	2	3	ωC–Cl (57)
38		240(w)	243	123	1	11	ωC–C (57)
39		215(w)	212	105	23	1	ωC–C (55)
40			198	85	4	5	ωC–N (57)
41			155	64	1	4	ωC–C (55)
42		120(s)	125	45	15	4	tCF3 (44)

Relative and absolute intensities of the experiments are abbreviated which includes: ν-stretching, sym-symmetric stretching, asym-asymmetric stretching, b-in-plane bending, ω-out-of-plane bending, ipb-in-plane bending, opb-out-of-plane bending, sb-symmetric bending, ipr-in-plane rock, opr-out-of-plane rock, t-torsion.

Table 9.2 The electric dipolemoment μ (Debye), average polarizabilityα_0 (×10^{-24}esu),anisotropy polarizability Δα(×10^{-24}esu), first hyperpolarizability β_0(×10^{-24}esu) and vector hyperpolarizability β_{vec}(×10^{-24}esu) for TFMBN calculated by B3LYP level with 6-311++G(d,p) basis set.

Parameters	B3LYP	Parameters	B3LYP
μ_x	–6.315	β_{xxx}	33.069
μ_y	4.317	β_{xxy}	31.673
μ_z	0.008	β_{xyy}	18.283
μ	8.548	β_{yyy}	15.295
α_{xx}	–73.325	β_{xxz}	-0.006
α_{xy}	–5.768	β_{xyz}	0.009
α_{yy}	-63.338	β_{yyz}	0.004
α_{xz}	0.007	β_{xzz}	–7.615
α_{yz}	0.005	β_{yzz}	–3.732
α_{zz}	–63.725	β_{zzz}	0.008
α_0	–47.643	β_0	8.179
Δα	18.615	β_{vec}	5.358

Table 9.3 Selected NBO results showing formation of Lewis and non-Lewis orbitals for TFMBNusing B3LYP/6-311++G(d,p) level of theory.

Bond (A–B)	ED/Energy (a.u)	(%) ED_A	(%) ED_B	NBO	(%) S	(%) P
σ(C7–N8)	1.988	47.43	63.72	$0.619(sp^{2.98})C+0.785(sp^{1.83})N$	43.03 57.47	84.89 74.56
σ(C7–N8)	1.917	57.45	63.68	$0.617(sp^{2.99})C+0.789(sp^{1.84})N$	33.09 44.48	75.79 65.56
σ(C12–F13)	1.925	47.56	53.41	$0.683(sp^{1.97})C+0.730(sp^{2.04})F$	47.57 33.68	67.34 63.85
π(C12–F14)	1.938	42.47	57.58	$0.651(sp^{1.00})C+0.758(sp^{1.00})F$	54.00 18.03	97.87 98.51
σ(C12–F15)	1.927	51.67	51.35	$0.698(sp^{2.99})C+0.716(sp^{4.80})F$	33.97 25.17	65.57 74.38

Table 9.4 Second order perturbation theory analysis ofFock matrix on NBO basis for TFMBN using B3LYP method with 6-311++G(d,p) basis set.+

Donor NBO (i)	Acceptor NBO (j)	$^{a}E^{(2)}$ (Kcal/mol)	$^{b}E(i)-E(j)$ (a.u)	$^{c}F(i,j)$ (a.u)
σ(C12–F13)	σ*(C4–C3)	2.54	2.25	0.047
	σ*(C5–C4)	2.81	2.26	0.053
σ(C12–F14)	σ*(C5–C6)	2.32	2.25	0.047
	σ*(C5–C4)	2.72	2.23	0.052
σ(C12–F15)	σ*(C2–C3)	2.27	2.26	0.047
	σ*(C3–C4)	2.74	2.24	0.043
σ(C7–N8)	σ*(C2–C1)	1.44	2.32	0.045
	σ*(C1–C6)	1.37	2.34	0.038
σ(C2–Cl9)	σ*(C2–C1)	5.97	2.51	0.035
	σ*(C2–C3)	4.69	0.59	0.045

$^{a}E^{(2)}$means energy of hyper conjugative interactions (stabilization energy).
^{b}Energy difference between donor and acceptor i and j NBO orbitals.
^{c}F(i,j) is the Fock matrix element between i and j NBO orbital.

Table 9.5 The experimental and calculated ^{13}C and ^{1}H NMR isotropic chemical shifts (δ in ppm) of TFMBN by B3LYP/6-311++G(d,p) method.

Atoms	δ ppm (Calculated)	δ ppm (Experimental)
C1	127.165	112
C2	114.248	116
C3	101.477	102
C4	115.139	108
C5	129.496	124
C6	82.943	70
C7	100.587	104
C12	105.265	114
H10	7.963	7.2
H11	7.524	7.0
H16	7.231	6.8

Table 9.6 Thermodynamic properties of DNB at different temperatures calculated by B3LYP/6-311++G(d,p) method.

Temperature (K)	Cp ($Calmol^{-1}K^{-1}$)	(H-E)/T ($KCalmol^{-1}$)	S ($KCalmol^{-1}$)	(G-E)/T ($KCalmol^{-1}$)
100	12.678	2.059	66.539	–74.527
200	21.975	6.827	72.797	–79.898
300	27.074	5.039	75.458	–83.648
400	38.269	7.976	83.854	–95.426
500	54.034	23.279	108.645	–103.871
600	58.376	28.157	116.569	–105.825
700	53.591	25.518	125.798	–117.341
800	72.495	31.571	135.992	–123.651
900	65.906	35.956	137.395	–129.452
1000	75.439	37.665	147.768	–135.205

Table 9.7 The Condensed fukui functions (f_k^+), (f_k^-), (f_k^0) considering Mulliken charges according with equation (12–14) for TFMBN obtained by B3LYP method.

Atoms	f_k^+	f_k^-	f_k^o
C1	0.0846	0.2067	0.0887
C2	0.0069	–0.0915	–0.0453
C3	–0.3536	–0.3589	–0.2905
C4	0.0768	–0.0652	–0.0073
C5	–0.3357	–0.2573	–0.2659
C6	0.0329	–0.0629	–0.0514
C7	–0.0356	–0.0625	–0.0423
C12	0.4165	0.2144	0.6591
H10	0.5456	0.1679	0.1996
H11	0.3561	0.1556	0.2134
H16	0.4515	0.3232	0.3276
N8	0.3962	0.3445	0.3495
Cl9	0.5079	0.3138	0.3179
F13	–0.4317	–0.2806	–0.2715
F14	0.8067	0.7516	0.7589
F15	0.8195	0.7529	0.7867